Turbulent mixing in a marginally-unstable shear layer

Hieu T. Pham[1], Sutanu Sarkar[1], William D. Smyth[2], and James N. Moum[2]

Department of Mechanical and Aerospace Engineering,
University of California, San Diego[1]
College of Earth, Ocean, and Atmospheric Science,
Oregon State University[2]
h8pham@ucsd.edu

Abstract

Large-eddy simulation (LES) is used to investigate turbulence in a marginally-unstable stratified shear layer motivated by the observation of deep-cycle turbulence in the upper Equatorial Undercurrents. The initial condition consists of uniform shear and stratification profiles, and a constant gradient Richardson number $Ri_g = 0.25$. A constant wind stress forces turbulence in the upper surface layer. Cases with different shear and stratification are simulated to elucidate the effects of shear and stratification on the deep-cycle turbulence. In all cases, a thin layer of enhanced shear rate descends from the surface into the stratified shear layer. As the layer deepens, it causes the local Ri_g to become less than 0.25, and shear instabilities develop into turbulence. Turbulent kinetic energy (TKE) in the shear layer is higher in cases with stronger shear, and it can be significantly larger than the TKE generated by the surface wind. Cases with stronger shear also have higher shear production, buoyancy flux, and dissipation rate in the TKE budget. The shear production is the largest term in the budget showing that the mean kinetic energy local to the shear layer is the main source of energy for turbulent mixing.

1 Introduction

Long-term observations in the Pacific Equatorial Undercurrent (EUC) indicate the consistent presence of night-time deep-cycle turbulence which occurs in the region well below the surface mixed layer (Moum et al., 1992; Peters et al., 1994; Lien et al., 2002). The phenomenon has ben shown to be related to marginally-stable condition of the Equatorial jet. The shear and stratification in this region is typically strong such that the local gradient Richardson number Ri_g fluctuates in a narrow range between 0.25 and 0.5. Due to this marginal stability condition, the flow can become unstable when it is triggered by surface processes. For example, Smyth et al. (2013) and Pham et al. (2013) show that a thin shear layer driven by surface wind descends into the region and causes the flow to become unstable.

Recent observational analysis shows that the marginally-unstable condition has seasonal variability (Smyth and Moum, 2013). Figure 1(a) illustrates how the values of Ri_g between 50 and 75 m depths influence the dissipation rate on a monthly basis. Overall, the dissipation rate is high when Ri_g falls in the marginally-stable range between $0.25 - 0.5$. In the months of April and May, Ri_g increases to a larger value and the dissipation rate is orders of magnitude smaller. During other months, although the values of Ri_g are similar, the dissipation rate in Fig. 1(a), the squared shear rate S^2 and the squared buoyancy frequency N^2 in Fig. 1(b) vary significantly from month to month. For example, the months of July and October have similar values of Ri_g but the shear, stratification and dissipation rate are notably larger in July. It is of interest to explore the physics behind the higher dissipation rate in order to parametrize the effects of deep-cycle turbulence in large-scale

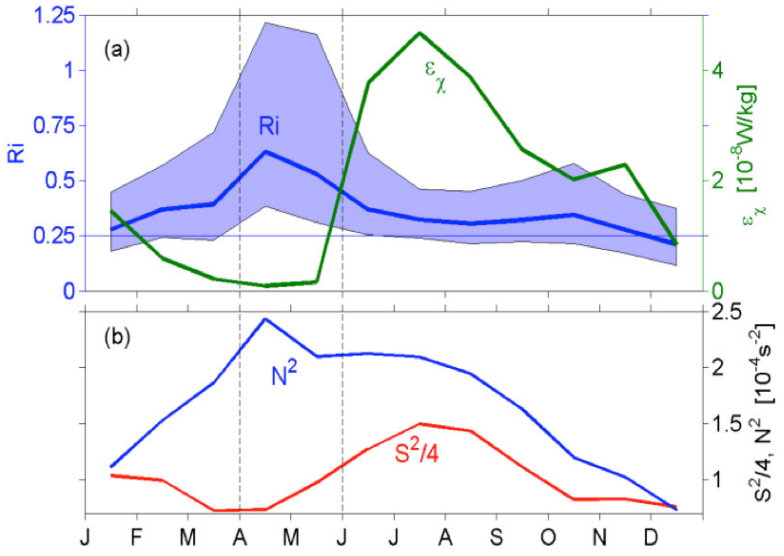

Figure 1: Seasonal variability of flow conditions at 60 m depth as observed in the Equatorial Undercurrents. Throughout the year, except for the months of April and May, the values Ri_g cluster in range of 0.25 to 0.5 showing the condition of marginal instability. Despite the narrow range of Ri_g, the values of shear and stratification change from season to season and so does the dissipation rate. See Smyth and Moum (2013) for further discussion on marginal instability.

ocean models. Well-known 1D turbulence models such as KPP parametrize eddy viscosity solely on local values of Ri_g, and therefore, may be inappropriate to represent deep-cycle turbulence.

Motivated by the observations in the EUC, we use LES to investigate the physics that governs turbulent mixing in a marginally-unstable stratified shear layer. In the numerical model, the shear rate and stratification in the shear layer are varied with Ri_g equal to 0.25. Our objective is to illustrate the differences in the evolution of the mean flow quantities and the turbulent kinetic energy budget during the onset of the deep-cycle turbulence in cases with different shear and stratification.

2 Model Formulation

We model the upper flank of the EUC jet as a stratified shear layer with the velocity and the temperature profiles that vary linearly with depth such that Ri_g is equal to 0.25 across the layer. Four cases with different shear and stratification are as shown in Fig. 2. In the figure, $S_0 = |d\langle u\rangle/dz|$ denotes the strength of the background shear rate where $\langle u\rangle$ is the horizontally-averaged zonal velocity. The subscript 0 indicates values at initial time. The shear layer spans the upper 100 m with a constant squared shear rate S^2. The profiles of N^2 have a $10\,m$ surface mixed layer below which N^2 is constant. The profiles of Ri_g are the same among cases and a constant wind stress $\tau_w = -0.052\,N\,m^{-2}$ is applied at the surface in all cases.

The numerical model integrates the three-dimensional non-hydrostatic Navier-Stokes equations under Boussinesq approximations in time. The model uses a 2^{nd}-order central finite-difference scheme in space and a 3^{rd}-order Runge-Kutta scheme in time. The pressure is computed using a multi-grid Poisson solver. The subgrid viscosity is computed using the LES subgrid model introduced in Ducros et al. (1996). The subgrid diffusivity is equal to the subgrid viscosity. The computational domain is $960\,m$ in the zonal (x)

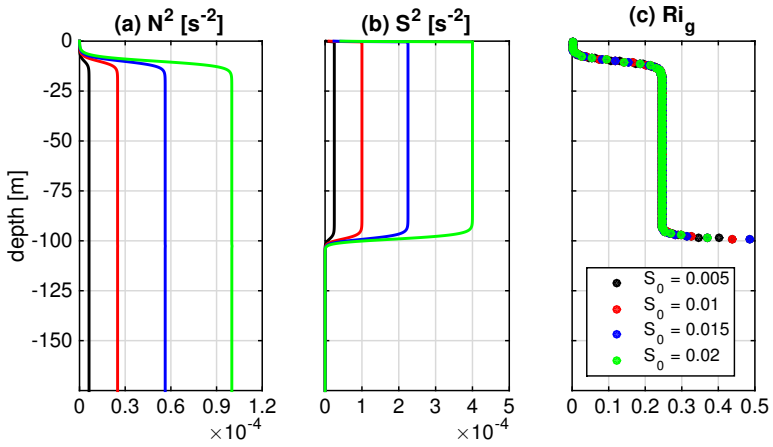

Figure 2: Profiles of initial squared buoyancy frequency N^2, squared shear rate S_0^2 and gradient Richardson number Ri_g for the four simulated cases. A constant wind stress $\tau_w = -0.052\,Nm^{-2}$ is applied at the surface in all cases.

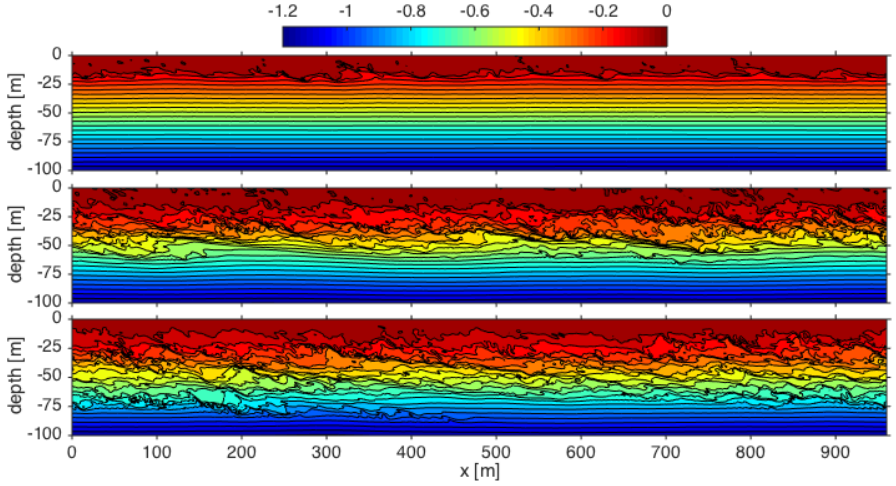

Figure 3: Snapshots of the temperature fields at three different times illustrate the evolution of turbulence as it spreads across the marginally-unstable shear layer in case $S_0 = 0.01s^{-1}$: (top) $t = 1.9\,hrs$, (middle) $t = 5.3\,hrs$, and (bottom) $t = 7.1\,hrs$. Turbulence deepens through a series of shear instability events.

direction, $80\,m$ in the meridional (y) direction and $260\,m$ in the vertical (z) direction. The grid spacing is $1.25\,m$ in the horizontal directions. In the top $100\,m$, the vertical grid spacing is $0.25\,m$, and it is stretched at a rate of 3% in the region below. A sponge region is set up in the bottom $100\,m$ to damp out reflected waves. Further details on the numerical methods can be found in Pham et al. (2013).

3 Results

3.1 Evolution of the marginally-unstable shear layer

In all cases, turbulence is initiated by the wind stress at the surface and spreads downward. Figure 3 illustrates three snapshots of the temperature field as the turbulence spreads into the shear layer in case $S_0 = 0.01s^{-1}$. At early time $t = 1.9\,hrs$, turbulence is confined to the top $20\,m$. The isothermals at this depth have corrugations resembling shear instabilities that bring colder fluid from below into the surface mixed layer. At $t = 5.3\,hrs$, the turbulent layer deepens down to $60\,m$ depth. The corrugated isotherms

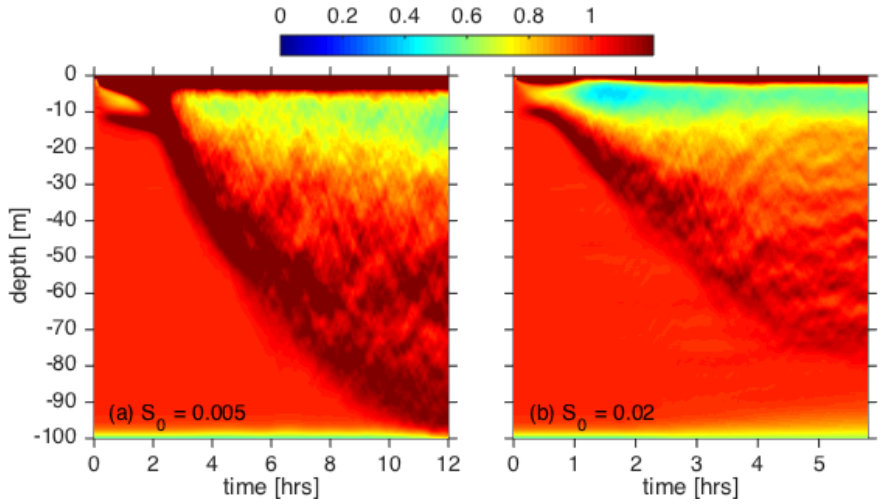

Figure 4: Evolution of the normalized squared shear rate $S^2/S_)^2$ in two cases. The turbulence is triggered by the descent of a thin layer with elevated shear from the surface. The elevated shear causes the local Ri_g to fall below 0.25 and triggers shear instabilities.

between depths of 25 and 60 m suggest shear instabilities with larger wavelength than those seen at earlier time. Isotherm overturns with the vertical scale of a few meters generate localized patches of turbulence. The turbulence reaches 90 m depth at $t = 7.1\,hrs$ with even larger isotherm overturns of approximately 10 m. A similar picture is seen in other cases: the turbulence spreads through multiple occurrences of shear instabilities that develop at the interface between the turbulent layer on the top and the quiescent shear layer in the region below.

The squared shear rate S^2 shown in Fig. 4 suggests how the shear layer becomes progressively turbulent. In all cases, as the wind generates turbulence in the surface mixed layer $z > -10\,m$, a thin layer of enhanced shear $S^2/S_0^2 > 1$ is formed in the region below. This layer of enhanced shear intrudes into the stratified layer triggering local shear instabilities and turbulence as was shown in Fig. 3. The deepening rate of the enhanced shear layer varies between the cases: faster spreading in cases with stronger shear and stronger stratification. In case $S_0 = 0.005\,s^{-1}$, the layer reaches 60 m depth after 5 hours while it takes only 3 hours to reach the same depth in case $S_0 = 0.02\,s^{-1}$. The faster spreading in cases with stronger shear suggests that the turbulence in the shear layer is controlled by the local shear rate and stratification, not by the gradient Richardson number.

The spreading of the turbulence across the shear layer creates multiple layers with alternating weaker and stronger shear. The layering is also seen in the profiles of stratification N^2. The thickness of the bands is comparable to the size of the overturns seen in Fig. 3. When an overturn mixes momentum and temperature in a localized patch of fluid, it causes the shear and stratification to increase in the vicinity immediately above and below the patch forming the bands. The layering also occurs in the profiles of Ri_g as shown in Fig. 5, and the similar trend is seen in all cases. The profiles in Figs. 5(a,b) show layers of fluctuating Ri_g with a vertical scale of about 10 m in the two cases $S_0 = 0.005$ and $0.02\,s^{-1}$ at different times as the turbulence spreads across the shear layer.

Despite the layering at the small vertical scale, the value of Ri_g in the case with weak shear $S_0 = 0.005\,s^{-1}$ in general tends to increase with depth. As the turbulence spreads across the shear layer, the local value of Ri_g is slightly reduced from the initial value of 0.25. The Ri_g profile at $t = 9.5\,hrs$ in Fig. 5(a) shows the layer between 50 and 100 m

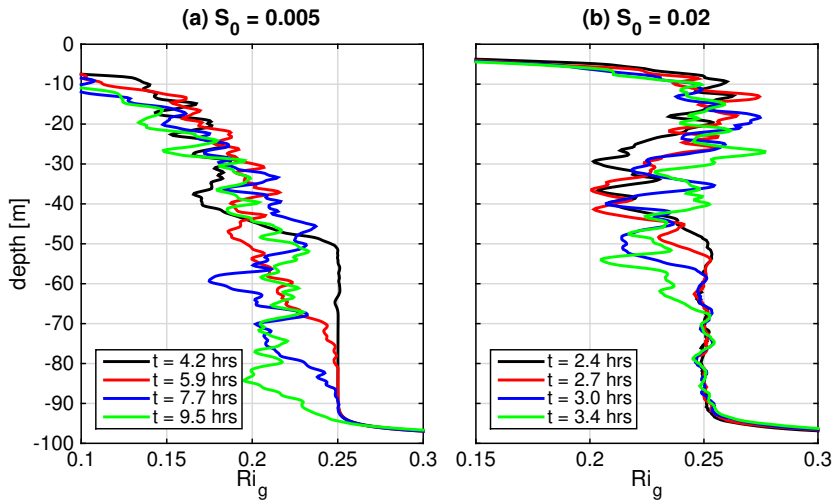

Figure 5: Profiles of Ri_g at different times in two cases: (a) $S_0 = 0.005\,s^{-1}$ and (b) $S_0 = 0.02\,s^{-1}$. The gradient Richardson reduces to slightly-smaller values when deep-cycle turbulence occurs.

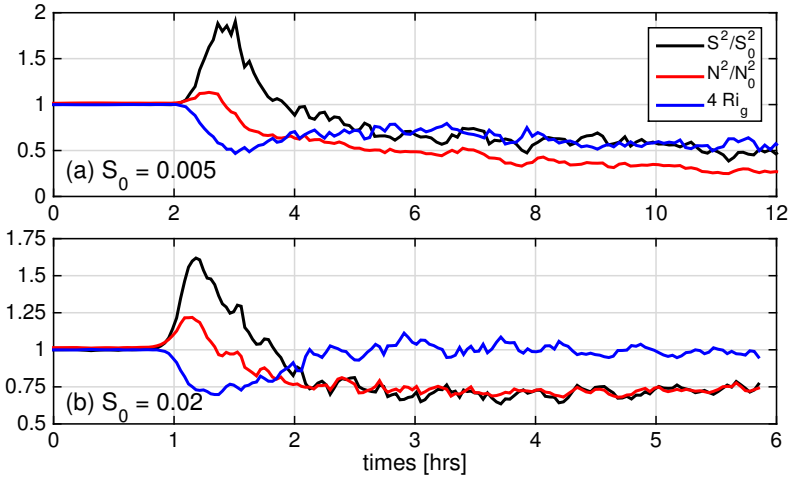

Figure 6: Evolution of N^2, S^2 and Ri_g at $20\,m$ depth in two cases: $(a) S_0 = 0.005\,s^{-1}$, and (b) $S_0 = 0.02\,s^{-1}$.

depth having a value of approximately 0.22 while the value is smaller in the region above. Fig. 5(b) shows the profiles in the case with stronger shear, $S_0 = 0.02\,s^{-1}$, and they are considerably different. The region between 30 and $50\,m$ depths has $Ri_g < 0.25$ while the region above, between 10 and $30\,m$ depths, has notably larger values that can exceed the critical value of 0.25.

Figure 6 illustrates how turbulence leads to the differences in the Ri_g profiles between the cases. The figure compares the temporal revolution of N^2, S^2 and Ri_g at $20\,m$ depth between the two cases: $S_0 = 0.005$ and $0.02\,s^{-1}$. In both cases, as the thin band of enhanced shear descends from the surface, the shear rate and the stratification at this depth increase; however, Ri_g decreases. As a result, shear instabilities develop into turbulence, and the shear and the stratification subsequently decrease. The difference between the two cases lies in the asymptotic value of Ri_g after the onset of turbulence. In the case $S_0 = 0.005\,s^{-1}$, Ri_g remains relatively small at the value of 0.125 which is small enough for turbulence to sustain at this depth. In contrast, Ri_g increases to 0.25 in

the case $S_0 = 0.02\,s^{-1}$ suggesting the decay of turbulence. After the onset of turbulence, the shear layer maintains a lower value of Ri_g in the case with weak shear and a larger value in the case with strong shear. The different values of Ri_g is due to the difference in turbulent mixing as will be discussed in the next section.

3.2 Evolution of turbulent kinetic energy

The background shear and stratification influence the intensity of turbulence generated in the shear layer. Figures 7 (a, b) contrast the profiles of turbulent kinetic energy between the cases with weakest and strongest S_0. When the shear is weak, the energy inside the shear layer is not as large as as the energy generated by the surface wind. The energy monotonically decreases with depth. However, the TKE profiles in the case with stronger shear show a peak inside the shear layer where shear instabilities develop. The energy inside the shear layer is considerably larger than the corresponding value in the surface layer. The trend among all cases is that increasing the initial shear and stratification increases the peak value of TKE inside the shear layer.

In the cases with stronger shear, the terms in the TKE budget also show larger values inside the shear layer. All terms in the budget shown in Fig. 7(d) for the case $S_0 = 0.02\,s^{-1}$ are larger than the terms in Fig. 7(c) for the case $S_0 = 0.005\,s^{-1}$. In the weak-shear case, the production shows a local peak inside the shear layer, but its value is smaller than the value at the surface. In the other case with strong shear, the peak production inside the shear layer is considerably larger than the value at the surface. Shear instabilities extract energy from local reservoir of mean kinetic energy and generates turbulence locally. While not shown, the Reynolds stresses $\langle u'w' \rangle$ also peak at the same depth as the production. The amplitude of the peak Reynolds stresses is larger in cases with stronger shear and it can be up to $5u_*^2$ in the case with strongest shear. The increase in production in the cases with larger S_0 is due to the larger mean shear and the larger Reynolds stress extracted through the development of shear instabilities. The dissipation rate and buoyancy flux also exhibit a similar trend as does the production.

Figure 7(e) plots the terms in the TKE budget integrated from the $20 - m$ depth downward in the case $S_0 = 0.005\,s^{-1}$, and it indicates that turbulence persists inside the layer until the end of the simulation at $t = 12\,hrs$. In contrast, the terms shown in Fig. 7(f) for the case $S_0 = 0.02\,s^{-1}$ initially increase but rapidly decay after a few hours. The integrated production peaks at time $t = 3.5\,hrs$ with a value of approximately 250 u_*^3 and then decreases to 20 u_*^3 at $t = 5.8\,hrs$. In the case with weak shear, the production sustains because the gradient Richardson number is less than 0.25 in the shear layer after the onset of turbulence as was previously shown in Fig. 5(a). The turbulence in the case with strong shear decays because Ri_g in the region right below the surface mixed layer in Fig. 5(b) attains values approximately equal to 0.25. The evolution of the integrated dissipation rate and buoyancy flux is similar to the production, and the turbulence decays faster in the cases with stronger shear. The large value of the integrated production, after scaling with u_*^3, further supports the result that the mean kinetic energy in the stratified shear layer contributes directly more to energizing turbulence at depth than the wind input.

4 Conclusions

Motivated by the observation of deep-cycle turbulence in the Equatorial Undercurrents, we use LES to investigate the evolution of turbulence inside a marginally-unstable

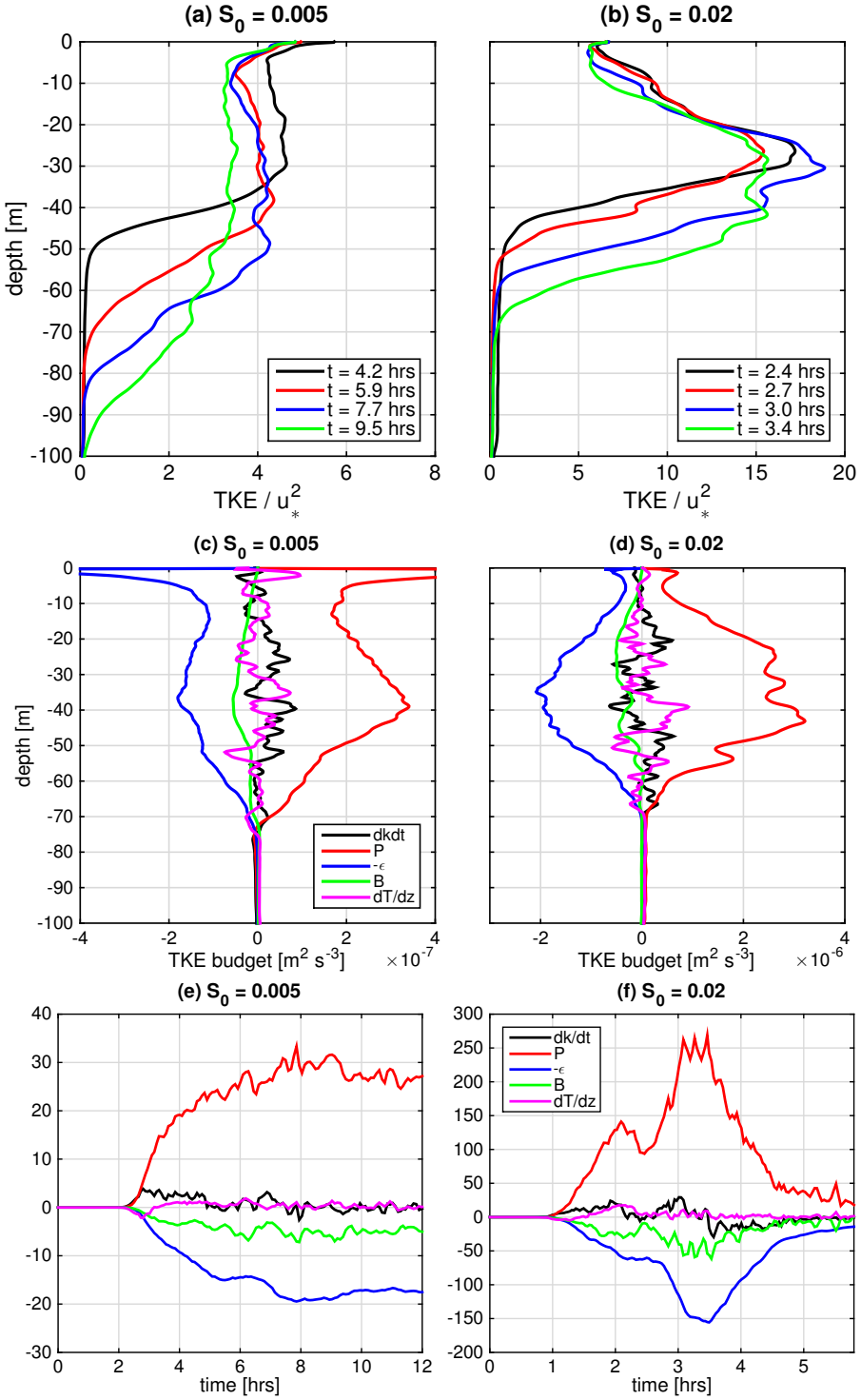

Figure 7: (a, b) The spread of turbulence illustrated through profiles of turbulent kinetic energy (TKE) at different times. The profiles are normalized by u_*^2. In panel (b), the peak k occurs in the EUC, not near the surface, showing the energy generated inside the stratified shear layer can be stronger than that generated by the wind. (c, d) Terms in the TKE budget: Tendency dk/dt, production P, dissipation ε, buoyancy flux B, and transport dT/dz. In panel (d), the production and dissipation in the shear layer are significantly larger than the corresponding values in the surface layer suggesting the local mean kinetic energy to be the major source of TKE. (e, f) Terms in the TKE budget integrated from 20 m depth down across the shear layer. The terms are scaled with u_*^3. Panels (a, c, e) are from the case $S_0 = 0.005\,s^{-1}$ and panels (b, d, f) are from the case $S_0 = 0.02\,s^{-1}$.

stratified shear layer. Initially, the shear and stratification are uniform and the gradient Richardson number is equal to 0.25. A constant wind stress is used to initiate turbulence. The initial shear and stratification are varied among cases to illustrate how the background condition affects the turbulence inside the layer.

In all cases, the shear layer becomes unstable due to the descent of a thin layer of enhanced shear from the surface. As the turbulence is initiated near the surface, it transports momentum downward. The transport causes the local shear rate to increase, the gradient Richardson number to decrease, and the flow becomes unstable to local shear instability. The turbulence continues to spread across the shear layer. The phenomenon of downward spreading of turbulence is the same in all simulated cases.

The values of background shear and stratification are found to affect the turbulence inside the shear layer despite all cases having the same gradient Richardson number. The turbulence in cases with stronger shear spreads across the shear layer at a faster rate. The main source of energy that is supplied to turbulence is found to be from the mean kinetic energy local to the shear layer.

The surface wind stress is the initiator of turbulence. But it is the reservoir of mean kinetic energy in the shear layer that is found to be the main source of turbulence at depth. There are qualitative differences in the evolution of TKE and Ri_g profiles between low- and high-shear cases. For example, TKE is larger at intermediate time but then decays in the high-shear case. The decay of turbulence seen in the cases with strong initial shear and stratification is transient and only occurs over a short time period of a few hours as observed in the EUC. Over a longer time scale, the shear and stratification in the shear layer will decrease and the turbulence will be sustained as seen in the cases with weak initial shear and stratification.

References

Ducros, F., P., C., and Lesieur, M. (1996). Lage-eddy simulation of transition to turbulence in a boundary layer developing spatially over a flat plate. *J. Fluid Mech.*, 326:1–36.

Lien, R.-C., D'Asaro, E., and McPhaden, M. (2002). Internal waves and turbulence in the upper central equatorial Pacific: Lagrangian and Eularian observations. *J. Phys. Oceanogr.*, 32:2619–2639.

Moum, J., Hebert, D., Paulson, C., and Caldwell, D. (1992). Turbulence and internal waves at the equator. Part I: Statistics from towed thermistors and a microstructure profiler. *J. Phys. Oceanogr.*, 22:1330–1345.

Peters, H., Gregg, M., and Sanford, T. (1994). The diurnal cycle of the upper equatorial ocean: Turbulence, fine-scale shear, and mean shear. *J. Geophys. Res.*, 99(C4):7707–7723.

Pham, H. T., Sarkar, S., and Winters, K. B. (2013). Large-eddy simulation of deep-cycle turbulence in an equatorial undercurrent model. *J. Phys. Oceanogr.*, 43:2490–2502.

Smyth, W. D. and Moum, J. N. (2013). Marginal instability and deep-cycle mixing in the eastern equatorial Pacific Ocean. *J. Geophys. Res.*, 40:6181–6185.

Smyth, W. D., Moum, J. N., Li, L., and Thorpe, S. A. (2013). Diurnal shear instability, the descent of the surface shear layer and the deep-cyle of equatorial turbulence. *J. Phys. Oceanogr.*, 43:2432–2455.